JOURNAL OF MATERIALS SCIENCE 35 (2000) 1339–1345

Transformation toughening of NiAl composites reinforced with yttria partially stabilized zirconia particles

M. LI
Department of Materials Science and Engineering, The Ohio State University, 2041 College Road, Columbus, OH 43210, USA

H. SCHAFFER
Instruments S.A., Inc., 3880 Park Avenue, Edison, NJ 08820, USA

W. O. SOBOYEJO
Princeton Materials Institute and Department of Mechanical and Aerospace Engineering, Princeton, NJ 08544, USA
E-mail: soboyejo@princeton.edu

The paper presents the results of a combined experimental and analytical study of transformation toughening in NiAl composites reinforced with 20 vol. % of 2 mole % yttria stabilized zirconia particles. The extent of stress-induced phase transformation is characterized using laser Raman spectroscopy techniques. The overall toughening increment due to stress-induced transformation is also predicted using micromechanics models that account for the role of dilatation only, or the combined effects of dilatation and shear.

1. Introduction

Since the pioneering work of Garvie *et al.* [1], transformation toughening in partially stabilized zirconia and zirconia toughened ceramics has been a subject of intensive study [1–12]. The studies have shown that the metastable tetragonal phase of zirconia can transform martensitically to monoclinic phase under an applied stress [1–12]. This stress-induced martensitic transformation is associated with a volume increase of approximately 3–5% (due to the lower density of the monoclinic phase) and can greatly enhance the fracture toughness of partially stabilized zirconia (PSZ), and brittle matrix composites reinforced with PSZ [1–12]. In both cases, a transformation zone is created as a crack propagates through a matrix reinforced with transforming particles, and a shielding stress is exerted on the crack (Fig. 1). This reduces the local stress intensity level at the crack tip, and thus improves the fracture toughness of the material.

Transformation toughening of NiAl has been studied by Barinov *et al.* [13–15], who showed that the fracture toughness of NiAl can be improved from a matrix fracture toughness of $\sim$15 MPa$\sqrt{\text{m}}$ to a fracture toughness of $\sim$25 MPa$\sqrt{\text{m}}$ after reinforcement with partially stabilized zirconia (PSZ) particles. They argued that the fracture toughness increment was due to transformation toughening on the basis of X-ray diffraction (XRD) analysis of the fracture surfaces and residual stress analysis. However, they did not conduct Raman spectroscopy and crack-tip transmission electron microscopy (TEM) studies to demonstrate conclusively the occurrence of the stress-induced phase transformation. Also, the NiAl matrix toughness that they measured in their studies was anomalously high ($\sim$15 MPa$\sqrt{\text{m}}$ compared with typical values of $\sim$4–7 MPa$\sqrt{\text{m}}$ reported by other researchers [16–19]).

Ramasundaram *et al.* [18] have also studied the NiAl composites reinforced with PSZ particles with different Y_2O_3 stabilization levels between (0 and 6 mole percent). They found significant toughness improvement (from a matrix value of 5.3 MPa$\sqrt{\text{m}}$ to a maximum of 14.1 MPa$\sqrt{\text{m}}$), especially in the NiAl/TZ-2Y (PSZ with 2 mole % Y_2O_3) composite. They also used Raman spectroscopy and TEM analysis to verify and quantify the occurrence of transformation toughening in the NiAl/TZ-2Y composite. The degree of transformation toughening was estimated using Raman spectroscopy measurements (of the spatial variation of the monoclinic phase content within the transformation zone) and micromechanics models that considered only dilatational stress-induced phase transformations. The predictions obtained from these models were generally lower than the measured toughening levels [16]. Also, transformation toughening was not detected in composites reinforced with unstabilized zirconia (no Y_2O_3), and PSZ containing 4 and 6 mole % Y_2O_3.

Zeng *et al.* [20] have developed discrete finite element models for the estimation of toughening due to purely dilatational stress-induced phase transformations. They modeled the same NiAl/TZ-2Y composite that was studied by Ramasundaram *et al.* [18], and predicted somewhat higher toughening levels than

TABLE I ΔK_T associated with transformation toughening (after Zeng *et al.* [17])

Toughness increment	Experimental data [16]	Theoretical predictions [7]	Hybrid finite element method	
			Uniform	Linear
ΔK_T (MPa$\sqrt{}$m)	9.0	3.5	3.7	6.2

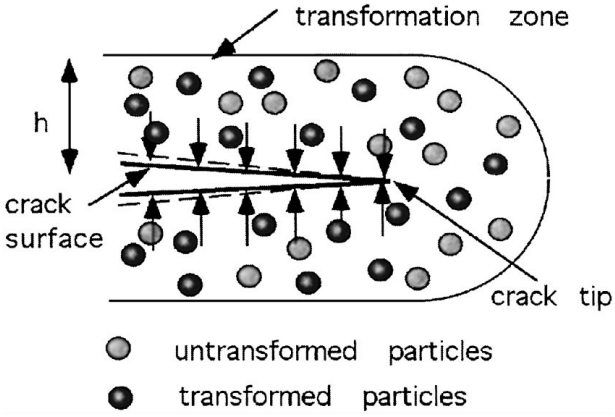

Figure 1 Schematic illustration of transformation toughening.

those obtained from the smeared-out dilatational models [7] that were used in the studies of Ramasundaram *et al.* [18]. However, they were unable to fully account for the measured toughening levels in the NiAl/TZ-2Y composites, as shown in Table I. Similar problems have been encountered by other researchers who have often found that the dilatational toughening models may not fully predict the measured toughening levels [6, 10, 18, 21, 22]. This suggests that the effects of shear stresses may also be important in the estimation of toughening due to stress-induced phase transformations.

Shear-induced phase transformations have been demonstrated by Chen and co-workers [21, 22] in MgO-stabilized and CeO-stabilized zirconia. Budiansky and Truskinovsky [23], Simha and Truskinovsky [24] and Stam and van der Giessen [25] have also modeled the effects of shear of the transformation toughening of zirconia ceramics. However, with the exception of prior work by Chen [21, 22], the authors of this paper are unaware of combined experimental and theoretical studies that explore the role of dilatation and shear in toughening of transformation toughened brittle matrix composites that do not have partially stabilized zirconia matrices.

The current paper presents the results of a combined experimental and theoretical study of transformation toughening on the fracture toughness/resistance-curve behavior of a model NiAl composite reinforced with 20 vol. % of 2 mole % yttria-partially stabilized zirconia. The extent of stress-induced phase transformation is characterized using laser Raman spectroscopy. The shielding effects of the stress-induced phase transformations are also estimated with analytical micromechanics models that assess the effects of dilatation and shear. As in previous studies [8, 10, 18, 21, 22], approximate dilatational models (with truncations of Taylor series expansions) are shown to underpredict the overall levels of transformation toughening. However, untruncated dilatational solutions provide better estimates of the overall toughening levels due to purely dilatational stress-induced martensitic phase transformations. The predictions obtained from untruncated dilatational plus shear solutions are also shown to be in reasonable agreement with experimentally-determined toughening levels, although these solutions somewhat overestimate the measured toughening levels. The untruncated dilatational solutions are shown to provide toughening estimates that are in almost exact agreement with the experimental data.

2. Materials

The −325 mesh (25–30 μm average size) NiAl powders were procured from Homogeneous Metals, Inc., Clayville, NY. The 2 mol. % yttria stabilized zirconia (YSZ) powders were obtained from Zirconia Sales, Marrietta, GA. The average particle size was approximately 0.35 μm. The NiAl and zirconia powders were mixed in suitable proportions, and ball milled using zirconia milling media for 24 hours. The resulting mixtures were transferred into stainless steel cans, before the cans were evacuated and sealed by electron beam welding. The evacuated and sealed cans were then hot isostatic pressed under 207 MPa pressure at 1100 °C for 4 hours.

The microstructure of the NiAl/YSZ composites is presented in Fig. 2. The zirconia phase occupies the grain boundary regions defined by the NiAl grains due to the large differences between the starting particles sizes of the NiAl (∼25 μm) and the zirconia (∼0.3 μm) powders. No porosity is observed. X-ray spectroscopy (XRD) and Raman spectroscopy analyses showed the zirconia phase in the composites is almost completely tetragonal. It is also important to note that all the YSZ particles are polycrystalline in nature. This

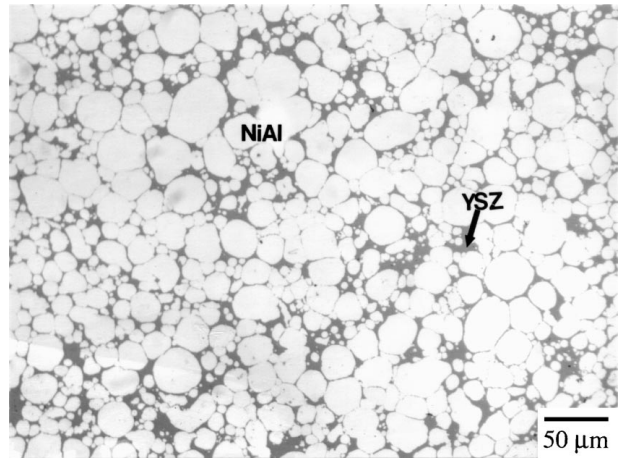

Figure 2 Typical microstructure of NiAl/YSZ composites.

has been demonstrated in prior TEM analysis of similar NiAl/YSZ composites which revealed that each of the YSZ agglomerates consists of particles/grains that are approximately 0.3–0.5 μm in diameter [18]. The YSZ particle sizes, which are the important microstructural scale for transformation toughening [4–6], were, therefore, much less than the agglomerate sizes in Fig. 2.

3. Experimental procedures

The initiation fracture toughness and the resistance-curve behavior of the NiAl/YSZ composites were studied using 38.1 mm long single edge notched bend (SENB) specimens with rectangular cross sections (15.24 mm width $\times$ 6.35 mm thickness). The specimens were fabricated via electro-discharge machining (EDM) with initial notch-length-to-width ratios of $\sim$0.25. The sides of the specimens were diamond polished prior to pre-cracking under cyclic compression [19]. After pre-cracking, the SENB specimens were loaded in incremental stages under three-point bending until crack initiation was observed from the pre-cracks. The loads were then increased in 2–5% increments to promote stable crack growth until specimen fracture occurred. The crack/microstructure interactions associated with stable crack growth were monitored with an optical microscope before and after each load increment. The fracture toughness of monolithic NiAl was also measured using SENB specimens with the same dimensions as the resistance-curve SENB specimens. These were used to determine the matrix toughness value. Fracture modes in the failed specimen were studied using scanning electron microscopy (SEM) techniques.

After fracture testing, micro Raman spectroscopy analysis was performed on the zirconia regions from the polished sides of the fractured SENB specimens [10, 18]. This was used to determine the volume fractions of monoclinic and tetragonal phases as functions of distance from the crack faces (up to a distance of $\sim$500 μm) [18]. Calibration procedures developed by Clarke and Adar [9] were used for the measurements of the volume fraction of the monoclinic phase. These utilize X-ray diffraction intensity measurements to arrive at an expression for the concentration of the monoclinic phase based on the monoclinic and tetragonal Raman peak intensities. The monoclinic phase concentration, (c_m), is thus given by:

$$c_m = \frac{I_m^{181} + I_m^{192}}{0.97\left(I_t^{148} + I_t^{264}\right) + I_m^{181} + I_m^{192}} \qquad (1)$$

where I refers to the integrated intensities of the peaks, the superscripts refer to the Raman shift of the peaks, and the subscripts m and t refers to the monoclinic and tetragonal peaks, respectively. Based on this expression, the volume fraction of monoclinic zirconia was determined as a function of distance from the fracture surface.

The Raman spectroscopy examination was performed partly at the Instruments S.A., Inc., Edison, NJ, and also in the Department of Chemistry at The Ohio State University, Columbus, OH. An argon ion laser beam with a probe diameter of $\sim$1 μm was used to excite the specimen. The microscope was equipped with a motion system and the scattered radiation was collected using a triple spectrometer. The initial Raman spectra were obtained from spots (on the sides of the specimens) that were very close to the fracture surfaces. The motion system was then used to guide the collection of spectroscopy data from points that were $\sim$2–3 μm apart. In this way, the volume fraction of transformed monoclinic phase was measured as a function of distance from the crack faces. The size of transformation zone was also estimated from the distance at which the volume fraction of transformed monoclinic phase was comparable to that in the bulk.

4. Results and discussion

4.1. Resistance-curve behavior and crack/microstructure interactions

The measured resistance-curve obtained for the NiAl/YSZ composite is presented in Fig. 3. This shows that the composite has an initiation toughness of $\sim$7.8 MPa$\sqrt{\text{m}}$. This initiation toughness is slightly higher than the matrix toughness, K_m, of NiAl of $\sim$6.6 MPa$\sqrt{\text{m}}$. The increase is due to the closure tractions associated predominantly with stress-induced phase transformations in the transformation zone behind the crack-tip of the fatigue pre-crack. These closure tractions give rise to an increase in the initiation toughness prior to the onset of crack growth. Subsequent resistance-curve behavior is strong, and the stress intensity factor required to promote stable crack growth increases rapidly until a steady-state toughness, K_{ss}, of $\sim$11.8 MPa$\sqrt{\text{m}}$ is approached. However, unstable crack growth and catastrophic failure ensued after $\sim$260 μm of stable crack growth.

The crack/microstructure interactions associated with the measured resistance-curve behavior are presented in Fig. 4. Stable crack growth and catastrophic failure of NiAl grains occurred predominantly by transgranular fracture, as is also evident from the fracture surface presented in Fig. 5. It is important to note here that stable crack growth (of the type observed in

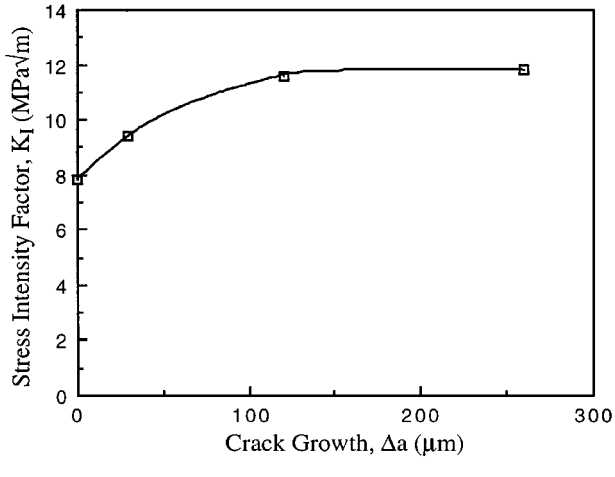

Figure 3 Experimental resistance-curve for NiAl/YSZ composites.

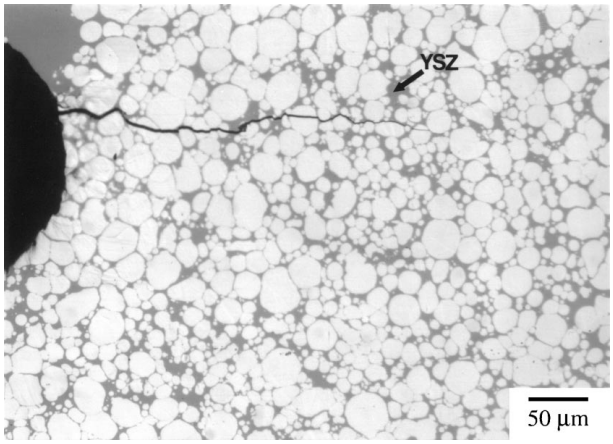

Figure 4 Stable crack growth in NiAl/YSZ composites.

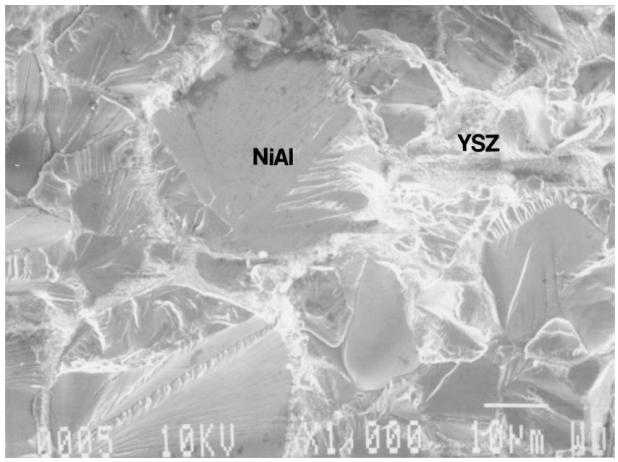

Figure 5 Typical fracture modes for NiAl/YSZ composites.

this study) has not been reported in monolithic NiAl, which generally undergoes unstable crack growth and intergranular fracture at an initiation toughness of ∼6–7 MPa$\sqrt{}$m [16–19]. The occurrence of stable crack growth in the NiAl/YSZ composite was therefore attributed to the beneficial effects of transformation induced "plasticity".

4.2. Raman spectroscopy analysis

In an effort to distinguish between monoclinic zirconia phase produced by the stress-induced transformation and that in the bulk, Raman spectroscopy analysis was performed on the bulk material far away from the crack faces, as well as material close to crack/fracture faces. The bulk volume fraction of transformed phase was thus determined using Equation 1. This was subtracted from the total volume fraction of monoclinic phase in the transformation zone, to obtain an estimate of the volume fraction of monoclinic phase produced by stress-induced phase transformation. The volume fraction of transformed phase, c, was thus estimated as a function of the distance from the crack face. The height of the transformation zone, h, was also estimated from the distance at which the volume fraction of transformed phase was found to be equal to the bulk volume fraction of tetragonal zirconia. In this way, two of the parameters that are critical to the modeling transformation toughening were determined for use in subsequent micromechanical modeling.

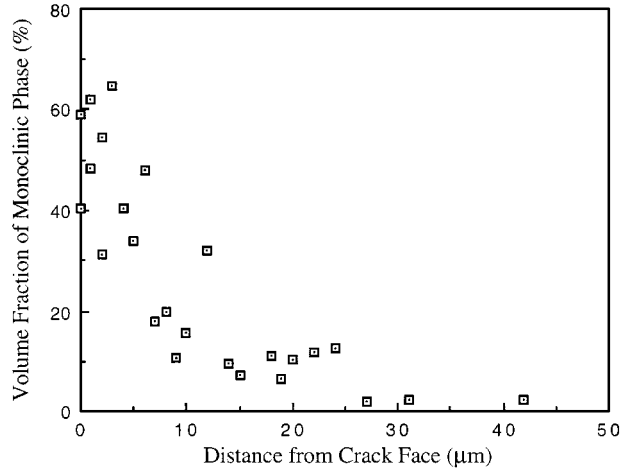

Figure 6 Volume fraction of monoclinic zirconia phase as a function of distance from crack face after final fracture.

The Raman spectroscopy analysis revealed that stress-induced phase transformations (from tetragonal to monoclinic phase) occurred in the zirconia particles close to the crack face. The results are shown in Fig. 6 in which the volume fraction of monoclinic phase is plotted as a function of distance from the crack face. As usual in transformation toughened materials [9, 10, 12, 18], there is a region of saturation close to the crack faces, and the volume fraction of transformed monoclinic phase decreases with increasing distance from the crack face (Fig. 6). Since the average volume percentage of transformed monoclinic phase in the bulk was ∼2%, we may estimate the size of the transformation zone to be ∼30 μm from Fig. 6. The average volume percentage of transformed monoclinic phase within the transformation zone may also be estimated to be ∼30%. Thus, the volume fraction of the zirconia undergoing transformation was estimated to be 0.06 (this is equal to the total volume fraction of zirconia of 0.2 multiplied by 30% of the particles that undergo stress-induced phase transformation in the transformation zone). These measured values will be used in the estimation of toughening components in the next section.

4.3. Toughening analysis

The toughening due to stress-induced martensitic transformations in YSZ particles, ΔK_{T}, may be estimated using the well known analysis of McMeeking and Evans [7] and Budiansky *et al.* [8]. For purely dilatational transformations, this gives [7, 8]:

$$\Delta K_{\mathrm{T}} = \frac{0.22 E_{\mathrm{c}} f \varepsilon_{\mathrm{c}}^{\mathrm{T}} \sqrt{h}}{1-\nu} \qquad (2)$$

where E_{c} is the composite modulus (∼191 GPa), f is the volume fraction of the zirconia undergoing transformation (∼0.06), $\varepsilon_{\mathrm{c}}^{\mathrm{T}}$ is the transformation strain (∼4%), h is the height of the transformation zone (∼30 μm) and ν is the Poisson's ration (∼0.3). Substituting the above

data into Equation 1, we may estimate the shielding contributions ΔK_T due to transformation toughening to be ~0.8 MPa$\sqrt{m}$. This clearly underestimates the overall toughening that was determined in the fracture toughness/resistance curve experiments, ΔK_{ex}, which is given by:

$$\Delta K_{ex} = K_{ss} - K_m \tag{3}$$

Since K_{ss} is 11.8 MPa$\sqrt{m}$ and K_m is 6.6 MPa$\sqrt{m}$, the overall toughness increment, ΔK_{ex}, is 5.2 MPa$\sqrt{m}$. Similar discrepancies have been reported by Ramasundaram *et al.* [18] and Zeng *et al.* [20] for NiAl/TZ-2Y (PSZ with 2 mol.% Y_2O_3) composites when toughening estimates were obtained using purely dilatational models as shown in Equation 2. A number of other researchers [8, 10, 21, 22] have also reported that the overall levels of transformation toughening in zirconia-toughened ceramics cannot be fully accounted for by micromechanical models than only account for the dilatational effects associated with volume changes due to the tetragonal-to-monoclinic stress-induced phase transformations.

This suggests than the role of shear must also be accounted for in the estimation of the overall toughening due to stress-induced phase transformations. The role of shear was neglected in much of the prior work because the orientations of the different shear variants were thought to effectively cancel each other out. However, work by Chen and co-workers [21, 22], Simha and Truskinovsky *et al.* [24], and Stam and van der Giessen [25] has shown that it is important to account for shear in the estimation of the overall toughening levels due to stress-induced phase transformations from tetragonal phase to monoclinic phase. The current paper will, therefore, explore a micromechanical modeling framework in which the roles of dilatational and shear stresses/strains will be investigated.

The approach that will be utilized is based on the work of Chen and co-workers [21, 22] and Evans *et al.* [26] who developed much of the fracture mechanics framework (for the estimation of transformation toughening) that is used in this paper. The work by Chen *et al.* [21, 22] established the basic mechanisms approach to the modeling of shear, while Evans *et al.* [26] proposed the use of the Hutchinson-Rice-Rosengreen (HRR) field expressions in the characterization of the complex stress and strain fields in the transformation zone.

Transformation toughening in this work, is attributed largely to the shielding effects provided by closure tractions in the transformation zone behind the crack-tip. These closure tractions can give rise to an increase in the fracture initiation toughness to levels that are greater than the matrix fracture toughness. This has been discussed in Section 4.1. The closure tractions associated with an evolving transformation zone can also give rise to resistance-curve behavior, as shown in Fig. 2, for the NiAl/PSZ composite that was examined in this study.

Furthermore, it is important to note here than the resistance-curve approaches a steady-state toughness,

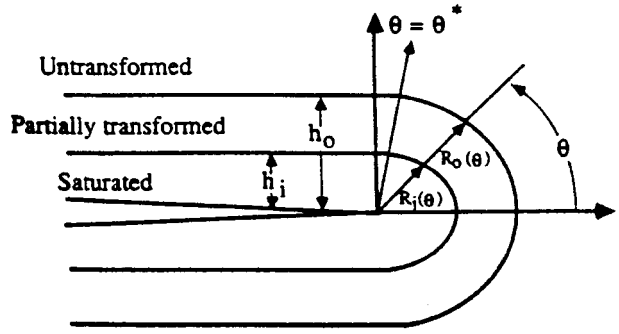

Figure 7 Crack-tip configuration showing the crack encircled by an inner zone of saturated transformation and an outer transitional zone of partial transformation (after Chen [22]). The outmost radius r is denoted by R, which coincides with h at $\theta = \theta^*$.

K_{ss}, as the crack length increases. This is associated with the evolution of a steady state process zone with a height, h_0 (Fig. 7). The process zone also includes a region with height h_i, where the transformation is saturated, and a partially transformed region between h_i and h_0 [19].

The overall toughening due to stress-induced phase transformations may be estimated from a simple energy balance [8]. This gives:

$$J = J_m + \Delta J = J_m + 2\int_0^{h_0} U(y)\,dy \tag{4}$$

where J is the J-integral, $U(y)$ is the energy per unit volume associated with loading and unloading cycle and ΔJ represents the toughness increment due to stress-induced phase transformations.

As discussed earlier, Evans *et al.* [26] have proposed that the stress-strain field within the transformation zone may be approximated with HRR field expressions. Hence, assuming a stationary crack (this is not really true for a growing crack in a resistance-curve test), ΔJ may be estimated to be [22]:

$$\Delta J = f\frac{2n}{n+1}h_0\sigma_0\varepsilon_0 \ln\left(\frac{h_0}{h_i}\right) \quad \text{for dilatational transformations} \tag{5}$$

or

$$\Delta J = f\frac{2n}{n+1}h_0\tau_0\gamma_0 \ln\left(\frac{h_0}{h_i}\right) \quad \text{for shear transformations} \tag{6}$$

where n is the inverse of the strain hardening exponent, σ_0 and τ_0 are the yield stresses in pure dilatation and pure shear, respectively, and ε_0 and γ_0 are the yield strains in pure dilatation and pure shear, respectively. Furthermore, from the strain expressions in the Ref. [22], we may obtain the following expressions:

$$\frac{h_i}{h_0} = \left(\frac{\sigma_0}{B\varepsilon_m^*}\right)^{(n+1)/n} \tag{7}$$

and

$$\frac{h_i}{h_0} = \left(\frac{\tau_0}{G\gamma_c^*}\right)^{(n+1)/n} \tag{8}$$

Substituting Equations 4 and 5 into Equations 2 and 3, respectively, gives:

$$\Delta J = 2 f h_0 \sigma_0 \left(\frac{\sigma_0}{G}\right) \ln\left(\frac{B\varepsilon_m^*}{\sigma_0}\right)$$
$$= 2 f h_0 \sigma_0 \left(\frac{\sigma_0}{G}\right) \ln\left(1 + \frac{B\varepsilon_m^T}{\sigma_0}\right) \tag{9}$$

and

$$\Delta J = 2 f h_0 \tau_0 \left(\frac{\tau_0}{G}\right) \ln\left(\frac{G\gamma_c^*}{\tau_0}\right)$$
$$= 2 f h_0 \tau_0 \left(\frac{\tau_0}{G}\right) \ln\left(1 + \frac{G\gamma_c^T}{\tau_0}\right) \tag{10}$$

For a weak transformation, we may estimate the overall toughening by considering only the first term in the Taylor series expansion for the logarithmic functions. This gives:

$$\Delta J = 2 f h_0 \sigma_0 \varepsilon_m^T \quad \text{for dilatational transformations} \tag{11}$$

and

$$\Delta J = 2 f h_0 \tau_0 \gamma_c^T \quad \text{for shear transformations} \tag{12}$$

Equations 11 and 12 are equivalent to relationships obtained from prior work by Budiansky *et al.* [8], and Chen and Reyes-Morel [18].

The toughness increments may be expressed in terms of the stress intensity factor, K, by using the standard relationship:

$$J = \frac{K^2}{E'} \tag{13}$$

where $E' = E$ for plane stress and $E' = E/(1-\nu^2)$ for plane strain conditions, E is the Young's modulus and ν is the Poisson's ratio. The resistance curve behavior may thus be estimated from:

$$K_c = K_m + \Delta K_T \tag{14}$$

where ΔK_T is the increment in fracture toughness due to stress-induced phase transformations, and K_c is the fracture toughness of the composite material.

Finally, for the current composite in which the transitional zone has been squeezed out, Chen [19] has shown that the overall toughening increment, ΔK, for weak transformations reduces to:

$$\Delta K = E_c' \varepsilon_m^T \sqrt{\alpha_m h_0} \quad \text{for dilatational transformations} \tag{15}$$

and

$$\Delta K = E_c' \gamma_c^T \sqrt{\alpha_c h_0} \quad \text{for shear transformations} \tag{16}$$

where

$$\alpha_m = \frac{\sqrt{3}(1+\nu)^2}{12\pi} \tag{17}$$

and

$$\alpha_c = \frac{1 + [2(1-2\nu)^2]/3}{8\pi} \tag{18}$$

Equation 15 is identical to prior expressions obtained by McMeeking and Evans [7] and Budiansky *et al.* [8] for pure dilatational transformations (Equation 2), while Equation 16 is equivalent to a prior expression by Chen and Reyes-Morel [18]. Substituting Equation 18 into Equation 16 gives the following equation for soft shear toughening:

$$\Delta K = \left[\frac{0.1614}{1-\nu}\right] \gamma_c^T E_c \sqrt{h} \quad \text{for plane strain} \tag{19}$$

Substituting $\gamma_c^T = 0.16$ into Equation 19, we may estimate the shielding contributions ΔK_T due to shear transformation toughening to be ~2.4 MPa$\sqrt{}$m. Hence, the soft shear toughening model does not fully account for the measured toughening of ~5.2 MPa$\sqrt{}$m in the NiAl/YSZ composites. Similarly, as stated earlier, the soft dilational model estimates the overall toughening to be ~0.8 MPa$\sqrt{}$m, which is well below the measured toughening level of ~5.2 MPa$\sqrt{}$m.

In contrast, the assumption of a strong transformation and the complete use of the terms in the logarithmic expressions in Equations 5, 6 and 13 leads to improved estimates of the overall toughening levels. From Fig. 6, the size of the saturated zone close to the crack-tip, h_i, can be estimated to be ~3 μm, while the overall size of the transformation zone, h_0, is ~30 μm. In the case of purely dilational transformations, the overall toughening levels, ΔK_T, may be estimated from Equation 5 (using data obtained by Chen for MgO-stabilized and Ceo-stabilized zirconia [21, 22]: $\varepsilon = 0.04$, $\sigma_0 = 500$ MPa, $\gamma_0 = 350$ MPa, $\tau_0 = 350$ MPa, and $n = 10$) to be ~5.4 MPa$\sqrt{}$m. For a matrix toughness of 6.6 MPa$\sqrt{}$m, this gives an overall prediction of composite toughness to be 12.0 MPa$\sqrt{}$m. This is in almost exact agreement with the measured steady state toughness of ~11.8 MPa$\sqrt{}$m at the end of the resistance-curve tests. The assumption of a strong transformation, therefore, improves the overall accuracy of the predicted toughening via the purely dilational model.

Similarly, in the case of dilation plus shear, the overall prediction of composite toughness may be estimated from Equation 6 to be 12.9 MPa$\sqrt{}$m. This somewhat overpredicts the measured steady state toughness. In any case, the predicted composite fracture toughness values are closer to the measured fracture toughness

levels when the complete expression for the toughening increments, ΔJ, are used in the estimation of toughening instead of the approximations from the Taylor series expressions. This indicates that some of the prior problems in the predictions of the overall shielding contributions from transformation toughening may be associated partly with the approximate nature of the expressions (truncated Taylor series etc.) that were used for the estimation of toughening [19]. The complete expressions for toughening due to strong transformations are, therefore, recommended for future modeling efforts.

5. Summary and concluding remarks

A combined experimental and theoretical study of transformation toughening of a NiAl/TZ-2Y composite has been carried out in this study. The following conclusions have been reached:

1. Stress-induced phase transformation occurs in the NiAl/YSZ composite during monotonic loading in resistance-curve experiments. The size of the saturated zone close to the crack-tip is $\sim$3 μm, while the overall size of the transformation zone is $\sim$30 μm. Laser Raman spectroscopy also provides estimates of the overall volume fraction of transformed monoclinic phase (due to stress-induced phase transformations) to be $\sim$0.06.

2. A simple analytical micromechanics framework is presented for the estimation of toughening due to pure dilatation, or dilatation plus shear. The framework includes approximate solutions (for weak transformations) obtained from Taylor series truncations, and complete analytical solutions obtained from "smeared out" models (for strong transformation).

3. The overall toughening due to stress-induced phase transformations in the NiAl/YSZ composite can only be fully predicted when the strong nature of the transformation is assessed within a micromechanics framework that does not include truncated Taylor series approximations. Predicted toughening levels from the untruncated dilational solutions are in closest agreement with the measured steady-state toughness levels.

Acknowledgements

The research is supported by the Division of Mechanics and Materials of the National Science Foundation with Dr. Dan Davis as Program Monitor. The authors are grateful to Dr. Davis for his encouragement and support.

References

1. R. C. GARVIE, R. H. HANNINK and R. T. PASCOE, *Nature* **258** (1975) 703.
2. D. J. GREEN, R. H. J. HANNINK and M. V. SWAIN, "Transformation Toughening of Ceramics," (CRC Press, Boca Raton, FL, 1989).
3. A. H. HEUER, N. CLAUSSEN, W. M. KRIVEN and M. RUHLE, *J. Amer. Ceram. Soc.* **65** (1982) 642.
4. F. F. LANGE, *J. Mater. Sci.* **17** (1982) 225.
5. P. F. BECHER, *Acta Metall.* **34** (1986) 1885.
6. A. G. EVANS and R. M. CANNON, *ibid.* **34** (1986) 761.
7. R. M. MCMEEKING and A. G. EVANS, *J. Amer. Ceram. Soc.* **65** (1982) 242.
8. B. BUDIANSKY, J. W. HUTCHINSON and J. C. LAMBROPOULOS, *Int. J. Solids Struct.* **19** (1983) 337.
9. D. R. CLARKE and F. ADAR, *J. Amer. Ceram. Soc.* **65** (1982) 284.
10. D. B. MARSHALL, M. C. SHAW, R. H. DAUSKARDT, R. O. RITCHIE, M. J. READEY and A. H. HEUER, *ibid.* **73** (1990) 2659.
11. M. L. MECARTNEY and M. RUHLE, *Acta Metall.* **37** (1989) 1859.
12. W. SOBOYEJO, D. BROOKS, L.-C. CHEN and R. LEDERICH, *J. Amer. Ceram. Soc.* **78** (1995) 1481.
13. S. M. BARINOV, V. YU. EVDOKIMOV and V. YA. SHEVCHENKO, *J. Mater. Sci. Lett.* **11** (1992) 1347.
14. S. M. BARINOV and V. YU. EVDOKIMOV, *Acta Metall. Mater.* **41** (1993) 801.
15. S. M. BARINOV, V. YU. EVDOKIMOV, V. F. PONOMAREV and V. YA. SHEVCHENKO, *J. Mater. Sci. Lett.* **13** (1994) 183.
16. D. B. MIRACLE, *Acta Metall. Mater.* **41** (1993) 649.
17. R. D. NOEBE, R. R. BOWMAN and M. V. NATHAL, *Int. Mater. Rev.* **38** (1993) 193.
18. P. RAMASUNDARAM, F. YE, R. R. BOWMAN and W. O. SOBOYEJO, *Metall. Mater. Trans. A* **29A** (1998) 493.
19. M. LI, R. WANG, N. KATSUBE and W. O. SOBOYEJO, *Scripta Mater.* **40** (1999) 397.
20. D. ZENG, N. KATSUBE and W. SOBOYEJO, *Comp. Mech.* in press.
21. I.-W. CHEN and P. E. REYES-MOREL, *J. Amer. Ceram. Soc.* **69** (1986) 181.
22. I.-W. CHEN, *ibid.* **74** (1991) 2564.
23. B. BUDIANSKY and L. TRUSKINOVSKY, *J. Mech. Phys. Solids* **41** (1993) 1445.
24. N. SIMHA and L. TRUSKINOVSKY, *Acta Metall. Mater.* **42** (1994) 3827.
25. G. TH. M. STAM and E. VAN DER GIESSEN, *Int. J. Solids. Struct.* **31** (1994) 1923.
26. A. G. EVANS, Z. B. AHMAD, D. G. GILBERT and P. W. R. BEAUMONT, *Acta Metall.* **34** (1986) 79.

Received 21 June
and accepted 19 August 1999